Chapter 2
An Introduction to the p- and hp-Versions of the Finite Element Method

The various methods described in this monograph for the computation of eigenpairs and GFIF/GSIFs cannot in general be carried out by means of analytical techniques; thus they require the use of numerical methods. We use the $p-$version of the FE method as the machinery for obtaining the required quantities, therefore, this chapter provides a brief introduction to these methods, their main features and characteristics. Readers interested in the mathematical aspects of $p-$ and $hp-$FEMs are encouraged to consult Schwab's book [157] whereas details on the applicative aspects of $p-$ and spectral FE methods are well documented in Karniadakis and Scherwin's book [92] and Szabó and Babuška's book [178].

2.1 The Weak Formulation

Let us consider the strong (or classical) formulation of the heat conduction equation in a two dimensional domain as the departing point, which is similar to (1.35) with Greek indices $\alpha, \beta = 1, 2$:

$$-\partial_\alpha \left(k_{\alpha\beta}\partial_\beta \tau\right) = Q \quad \text{in } \Omega \in \mathbb{R}^2. \tag{2.1}$$

For ease of explanation let us assume that homogeneous Dirichlet boundary conditions are specified on a part of the boundary $\partial\Omega_D$, and Neumann boundary conditions on the rest of the boundary $\partial\Omega_N = \partial\Omega/\partial\Omega_D$:

$$\tau = 0 \quad \text{on } \partial\Omega_D, \tag{2.2}$$

$$([k]\mathbf{grad}\tau)\cdot\mathbf{n} = \hat{q}_n \quad \text{on } \partial\Omega_N. \tag{2.3}$$

The Dirichlet boundary condition (2.2) is called an "essential" boundary condition, whereas the Neumann boundary condition (2.3) is called a "natural" boundary

Z. Yosibash, *Singularities in Elliptic Boundary Value Problems and Elasticity and Their Connection with Failure Initiation*, Interdisciplinary Applied Mathematics 37,
DOI 10.1007/978-1-4614-1508-4_2, © Springer Science+Business Media, LLC 2012

condition. Multiplying (2.1) by a function $\chi(x_1, x_2)$, chosen to satisfy the "essential" boundary conditions, i.e., $\chi = 0$ on $\partial\Omega_D$, and integrating over Ω, one obtains

$$-\int_\Omega \chi\ \partial_\alpha \left(k_{\alpha\beta}\partial_\beta \tau\right) d\Omega = \int_\Omega \chi\ Q\ d\Omega. \tag{2.4}$$

Applying Green's theorem to the left-hand side of (2.4), one obtains

$$-\int_\Omega \chi\ \partial_\alpha \left(k_{\alpha\beta}\partial_\beta \tau\right)\ d\Omega = -\int_{\partial\Omega} \chi\, k_{\alpha\beta}\partial_\beta \tau n_\alpha\ d\Gamma + \int_\Omega k_{\alpha\beta}\ \partial_\beta\tau\ \partial_\alpha\chi\ d\Omega. \tag{2.5}$$

Because χ is zero on $\partial\Omega_D$, the boundary integral in (2.5) reduces to the boundary $\partial\Omega_N$, on which we can use (2.3). Thus the left-hand side of (2.4) becomes

$$-\int_{\partial\Omega_N} \chi\hat{q}_n\ d\Gamma + \int_\Omega k_{\alpha\beta}\ \partial_\beta\tau\ \partial_\alpha\chi\ d\Omega. \tag{2.6}$$

Inserting (2.6) into (2.4), one obtains

$$\int_\Omega k_{\alpha\beta}\ \partial_\beta\tau\ \partial_\alpha\chi\ d\Omega = \int_\Omega \chi\ Q\ d\Omega + \int_{\partial\Omega_N} \chi\hat{q}_n\ d\Gamma. \tag{2.7}$$

What has been obtained in (2.7) is the weak formulation already presented in (1.37) in a 3-D setting, where the left-hand side is denoted the bilinear form $\mathcal{B}(\tau, \chi)$ (see (1.38)), and the right-hand side is denoted by the linear form $\mathcal{F}(\chi)$ (see (1.39)). In summary, the weak formulation for this example problem is

$$\text{Seek } \tau_{\text{EX}} \in \mathcal{E}_o(\Omega) \text{ such that} \qquad \mathcal{B}(\tau_{\text{EX}}, \chi) = \mathcal{F}(\chi) \qquad \forall\, \chi \in \mathcal{E}_o(\Omega), \tag{2.8}$$

with $\mathcal{E}_o(\Omega) = \{\tau(x_1, x_2) \mid \tau \in \mathcal{E}(\Omega),\ \tau = 0 \text{ on } \partial\Omega_D\}$ and $\mathcal{E}(\Omega)$ is defined in Appendix A.

It can be shown that the weak formulation is equivalent to the principle of minimum potential energy (see, for example, [178]). Define the potential energy (a functional) by

$$\Pi(\tau) \overset{\text{def}}{=} \frac{1}{2}\mathcal{B}(\tau, \tau) - \mathcal{F}(\tau). \tag{2.9}$$

The principle of minimum potential energy states that the exact solution is the one that gives the potential energy a minimum value:

$$\Pi_{\text{EX}} \overset{\text{def}}{=} \Pi(\tau_{\text{EX}}) = \min_{\chi\in\mathcal{E}(\Omega)} \Pi(\chi). \tag{2.10}$$

Of course, if essential boundary conditions are prescribed, the energy space has to be adjusted accordingly. The main role of the potential energy principle is its use

in estimating the error of the approximated FE solution, and in understanding the concept of monotonic convergence when using hierarchical spaces (which will be discussed in the next subsection).

2.2 Discretization

As formulated, $\mathcal{E}_o(\Omega)$ is an infinitely large space, so that in order to solve (2.8), one needs to find a function within an infinite number of functions. This is, of course, not practically possible. Instead, and *this is the major step where the discretization errors are introduced*, one may consider a finite-dimensional subspace, i.e., in $\mathcal{E}_o^N(\Omega) \subset \mathcal{E}_o(\Omega)$, such that $\dim(\mathcal{E}_o^N) = N$. So instead of solving (2.8), we are seeking an approximate solution, denoted by $\tau_{\text{FE}} \in \mathcal{E}_o^N(\Omega)$:

$$\text{Seek } \tau_{\text{FE}} \in \mathcal{E}_o^N(\Omega), \text{ such that } \quad \mathcal{B}(\tau_{\text{FE}}, \chi) = \mathcal{F}(\chi) \qquad \forall \chi \in \mathcal{E}_o^N(\Omega). \tag{2.11}$$

One important property is that from all functions in $\mathcal{E}_o^N(\Omega)$, the function τ_{FE} that satisfies (2.11) is the closest to τ_{EX} when measured in the *energy norm*:

$$\min_{\tau \in \mathcal{E}_o^N(\Omega)} \|\tau_{\text{EX}} - \tau\|_{\mathcal{E}_o^N(\Omega)} = \|\tau_{\text{EX}} - \tau_{\text{FE}}\|_{\mathcal{E}_o^N(\Omega)}, \tag{2.12}$$

and furthermore, the numerical error $e(\boldsymbol{x}) \overset{\text{def}}{=} \tau_{\text{EX}} - \tau_{\text{FE}}$ is orthogonal to the space $\mathcal{E}_o^N(\Omega)$. The important question that arises is, how can one estimate the numerical error $e(\boldsymbol{x})$? The answer to this question requires the definitions of hierarchical spaces and extensions.

Consider, for example, a set of hierarchical subspaces (see a graphical interpretation of hierarchical subspaces as opposed to non-hierarchical subspaces in Figure 2.1) $\mathcal{E}_o^{N_1}(\Omega) \subset \mathcal{E}_o^{N_2}(\Omega) \subset \cdots \subset \mathcal{E}_o(\Omega)$, having the property that

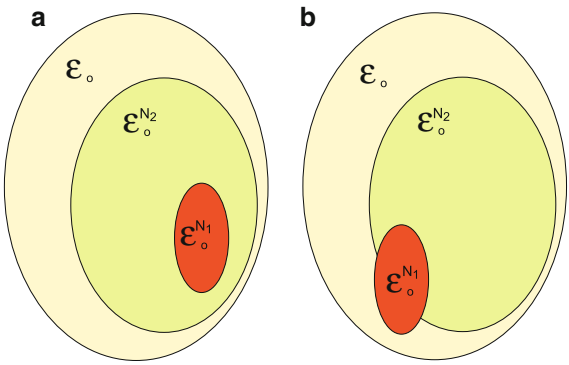

Fig. 2.1 **(a)** Hierarchical as opposed to **(b)** non-hierarchical subspaces.

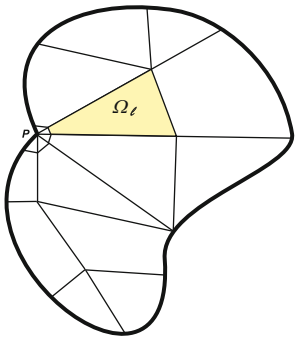

Fig. 2.2 A typical 2-D FE p-mesh.

$N_1 < N_2 < \cdots$. Then by (2.12), $\|\tau_{\text{EX}} - \tau_{\text{FE}_2}\|_{\mathcal{E}_o(\Omega)} \leq \|\tau_{\text{EX}} - \tau_{\text{FE}_1}\|_{\mathcal{E}_o(\Omega)}$. Of course, as the space $\mathcal{E}_o^N(\Omega)$ is enriched by more and more functions, then the approximated solutions become closer to the exact solution. The systematic enrichments of the subspaces are called *extensions*, and we will elaborate on a special extension procedure, called p- and hp-extensions.

In order to solve (2.8), we partition the domain over which the integration has to be performed into quadrilateral or triangular subdomains, called *elements*. The collection of these elements is called the FE "mesh." Each element is denoted by Ω_ℓ, so that $\cup\Omega_\ell = \Omega$; see Figure 2.2 as an example of a typical FE p-mesh. Having the mesh, the integral over the entire domain can be replaced by the sum of integrals over each subdomain (element), so that the weak form in (2.8) can now be stated as

$$\text{Seek } \tau_{\text{FE}} \in \mathcal{E}_o^N(\Omega), \text{ such that } \quad \sum_\ell \mathcal{B}_\ell(\tau_{\text{FE}}, \chi) = \sum_\ell \mathcal{F}_\ell(\chi) \qquad \forall \chi \in \mathcal{E}_o^N(\Omega), \tag{2.13}$$

where $\mathcal{B}_\ell(\tau, \chi)$, for example, is the bilinear form over the element Ω_ℓ,

$$\mathcal{B}_\ell(\tau, \chi) = \int_{\Omega_\ell} k_{\alpha\beta}\, \partial_\beta \tau\, \partial_\alpha \chi\, d\Omega = \iint_{\Omega_\ell} \left(\frac{\partial \chi}{\partial x_1} \quad \frac{\partial \chi}{\partial x_2} \right) \begin{bmatrix} k_{11} & k_{12} \\ k_{12} & k_{22} \end{bmatrix} \begin{Bmatrix} \frac{\partial \tau}{\partial x_1} \\ \\ \frac{\partial \tau}{\partial x_2} \end{Bmatrix} dx_1 dx_2, \tag{2.14}$$

and the linear form for the element is

$$\mathcal{F}_\ell(\chi) = \iint_{\Omega_\ell} \chi Q\, dx_1 dx_2 + \int_{\partial\Omega_{N\ell}} \chi \hat{q}_n d\Gamma. \tag{2.15}$$

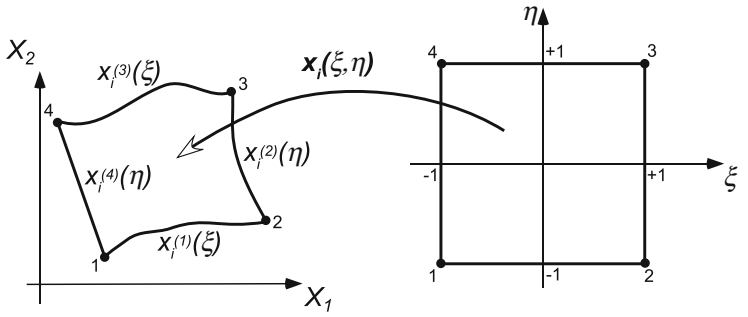

Fig. 2.3 Blending mapping from the standard element to the "physical" element.

2.2.1 *Blending Functions, the Element Stiffness Matrix and Element Load Vector*

Integrating over different-shaped quadrilaterals and triangles is a complicated procedure. To overcome this difficulty, a standard element is introduced. Assume that one needs to evaluate (2.14) over the quadrilateral domain shown in the left side of Figure 2.3, where the sides of the element have parametric representations. In view of Figure 2.3, we denote by $x_i^{(j)}(t)$, $-1 \le t = \xi, \eta \le 1$, the parametric representation of the curved edge j and by $X_i^{(j)}$ the coordinates of vertex j. With these definitions and using the "blending function method"[68], it is possible to "map" the standard quadrilateral element $\Omega_{st}^{Q} = \{(\xi,\eta) \mid -1 \le \xi \le 1,\ -1 \le \eta \le 1\}$ into any quadrilateral element with curved boundaries Ω_{ℓ}^{Q}:

$$
\begin{aligned}
x_i(\xi,\eta) = {} & \frac{1}{2}(1-\eta)x_i^{(1)}(\xi) + \frac{1}{2}(1+\xi)x_i^{(2)}(\eta) + \frac{1}{2}(1+\eta)x_i^{(3)}(\xi) \\
& + \frac{1}{2}(1-\xi)x_i^{(4)}(\eta) \\
& - \frac{1}{4}(1-\xi)(1-\eta)X_i^{(1)} - \frac{1}{4}(1+\xi)(1-\eta)X_i^{(2)} \\
& - \frac{1}{4}(1+\xi)(1+\eta)X_i^{(3)} - \frac{1}{4}(1-\xi)(1+\eta)X_i^{(4)}, \quad i = 1,2. \qquad (2.16)
\end{aligned}
$$

With the aid of the blending functions, one has

$$
\begin{Bmatrix} \frac{\partial}{\partial\xi} \\ \\ \frac{\partial}{\partial\eta} \end{Bmatrix} = [J] \begin{Bmatrix} \frac{\partial}{\partial x_1} \\ \\ \frac{\partial}{\partial x_2} \end{Bmatrix}, \quad \text{with} \quad [J] = \begin{bmatrix} \frac{\partial x_1}{\partial\xi} & \frac{\partial x_2}{\partial\xi} \\ \frac{\partial x_1}{\partial\eta} & \frac{\partial x_2}{\partial\eta} \end{bmatrix},
$$

so the bilinear form for element ℓ is

$$\mathcal{B}_\ell(\tau,\chi)=\iint_{-1}^{1}\left(\frac{\partial\chi}{\partial\xi}\ \frac{\partial\chi}{\partial\eta}\right)\left([J]^{-1}\right)^T[k]\left([J]^{-1}\right)\left\{\begin{array}{c}\frac{\partial\tau}{\partial\xi}\\ \\ \frac{\partial\tau}{\partial\eta}\end{array}\right\}|J|d\xi d\eta. \tag{2.17}$$

Similarly, if for example the boundary of the domain coincides with the element edge 2-3 (see Figure 2.3), then the linear form for element ℓ is

$$\mathcal{F}_\ell(\chi)=\iint_{-1}^{1}\chi Q\ |J|d\xi d\eta+\int_{-1}^{1}(\chi\hat{q}_n)\,|_{\xi=1}d\eta. \tag{2.18}$$

2.2.2 The Finite Element Space

There are three ways of increasing the FE space, i.e., there are three different extension possibilities:

1. *h-Extension:* Refining the FE mesh (i.e., adding more elements), while keeping over each element a basis consisting of a given number of functions.
2. *p-Extension:* Keeping the FE mesh fixed and increasing the number of basis functions over each element.
3. *hp-Extension:* Changing the mesh and the number of basis functions over individual or all elements.

A necessary condition for a function to be in $\mathcal{E}(\Omega)$ is that it be C^0 continuous, i.e., continuity across elements' boundaries is maintained. Instead of defining a basis function over the entire Ω, we define a set of element basis functions, so that on combining all together, they provide a C^0 continuous overall function. Since the weak formulation has been split into a sum over all elements, and furthermore, all integrations are performed over the standard element, it is only natural to define a basis function for approximating both the test and trial functions on the standard element.

Let the trial function τ and the test function χ be expressed in terms of an elemental basis functions $\Phi_i(\xi,\eta)$ (spanning a finite-dimensional subspace) in the standard element

$$\tau(\xi,\eta)=\sum_{i=1}^{DOF}b_i^{(\ell)}\Phi_i(\xi,\eta)=\boldsymbol{\Phi}^T\boldsymbol{b}^{(\ell)}\qquad \chi(\xi,\eta)=\sum_{i=1}^{DOF}c_i^{(\ell)}\Phi_i(\xi,\eta)=(\boldsymbol{c}^{(\ell)})^T\boldsymbol{\Phi}, \tag{2.19}$$

where $b_i^{(\ell)}$ and $c_i^{(\ell)}$ are the amplitudes of the basis functions in element ℓ, and Φ_i are products of integrals of Legendre polynomials in ξ and η. Substituting (2.19) into (2.17), one obtains an expression for the unconstrained elemental stiffness

matrix $[K^{(\ell)}]$ associated with $\mathcal{B}_\ell$;

$$\mathcal{B}_\ell(\tau, \chi) = (\boldsymbol{c}^{(\ell)})^T [K^{(\ell)}] \boldsymbol{b}^{(\ell)}, \tag{2.20}$$

and the entries of $[K^{(\ell)}]$ are computed by

$$K_{ij}^{(\ell)} = \iint_{-1}^{1} \left(\frac{\partial \Phi_i}{\partial \xi} \; \frac{\partial \Phi_i}{\partial \eta} \right) \left([J]^{-1} \right)^T [k] \left([J]^{-1} \right) \begin{Bmatrix} \frac{\partial \Phi_j}{\partial \xi} \\ \\ \frac{\partial \Phi_j}{\partial \eta} \end{Bmatrix} |J| d\xi d\eta. \tag{2.21}$$

Substituting (2.19) into (2.18), one obtains an expression for the unconstrained load vector $\boldsymbol{r}^{(\ell)}$ associated with $\mathcal{F}_\ell$;

$$\mathcal{F}_\ell(\chi) = (\mathbf{c}^{(\ell)})^T \boldsymbol{r}^{(\ell)}, \tag{2.22}$$

and the entries of $\boldsymbol{r}^{(\ell)}$ are computed by

$$r_i^{(\ell)} = \iint_{-1}^{1} \Phi_i \, Q \, |J| d\xi d\eta + \int_{-1}^{1} (\Phi_i \hat{q}_n) \, |_{\xi=1} d\eta. \tag{2.23}$$

Hierarchic Basis (Shape) Functions for Quadrilateral Elements

There are many possibilities for choosing a basis of functions to span the space $\mathcal{E}^N$. Usually it is constructed by specially chosen polynomials based on Legendre or Jacobi polynomials (see for example [32,91,178]). Here we present shape functions for the classical h-version of the FEMs and a family of hierarchical shape functions over quadrilateral elements for the p-version of the FEM, as described in [178], based on the Legendre polynomials. This basis function is extendable to triangular elements also (details are provided in [91, 178]).

Conventional Parabolic (second-order) h-Space

Serendipity (8-nodes)

Vertex

$$\Phi_1(\xi, \eta) = -\frac{1}{4}(1-\xi)(1-\eta)(1+\xi+\eta)$$

$$\Phi_2(\xi, \eta) = -\frac{1}{4}(1+\xi)(1-\eta)(1-\xi+\eta)$$

$$\Phi_3(\xi, \eta) = -\frac{1}{4}(1+\xi)(1+\eta)(1-\xi-\eta)$$

$$\Phi_4(\xi, \eta) = -\frac{1}{4}(1-\xi)(1+\eta)(1+\xi-\eta)$$

Product (9-nodes)

Vertex

$$\Phi_1(\xi, \eta) = \frac{1}{4}\xi\eta(\xi-1)(\eta-1)$$

$$\Phi_2(\xi, \eta) = \frac{1}{4}\xi\eta(\xi+1)(\eta-1)$$

$$\Phi_3(\xi, \eta) = \frac{1}{4}\xi\eta(\xi+1)(\eta+1)$$

$$\Phi_4(\xi, \eta) = \frac{1}{4}\xi\eta(\xi-1)(\eta+1)$$

Edge

$$\Phi_5(\xi,\eta) = \frac{1}{2}\left(1-\xi^2\right)(1-\eta)$$

$$\Phi_6(\xi,\eta) = \frac{1}{2}(1+\xi)\left(1-\eta^2\right)$$

$$\Phi_7(\xi,\eta) = \frac{1}{2}\left(1-\xi^2\right)(1+\eta)$$

$$\Phi_8(\xi,\eta) = \frac{1}{2}(1-\xi)\left(1-\eta^2\right)$$

Edge

$$\Phi_5(\xi,\eta) = \frac{1}{2}\left(1-\xi^2\right)\eta(\eta-1)$$

$$\Phi_6(\xi,\eta) = \frac{1}{2}\left(1-\eta^2\right)(1+\xi)$$

$$\Phi_7(\xi,\eta) = \frac{1}{2}\left(1-\xi^2\right)(1+\eta)$$

$$\Phi_8(\xi,\eta) = \frac{1}{2}(1-\eta)\xi(\xi-1)$$

Face

$$\Phi_9(\xi,\eta) = \left(1-\xi^2\right)\left(1-\eta^2\right)$$

Hierarchical (p-version) Trunk Space

Vertex

$$\Phi_1(\xi,\eta) = \frac{1}{4}(1-\xi)(1-\eta)$$

$$\Phi_2(\xi,\eta) = \frac{1}{4}(1+\xi)(1-\eta)$$

$$\Phi_3(\xi,\eta) = \frac{1}{4}(1+\xi)(1+\eta)$$

$$\Phi_4(\xi,\eta) = \frac{1}{4}(1-\xi)(1+\eta)$$

Edge

$$\Phi_5(\xi,\eta) = -\sqrt{\frac{3}{32}}\left(1-\xi^2\right)(1-\eta)$$

$$\Phi_6(\xi,\eta) = -\sqrt{\frac{3}{32}}(1+\xi)\left(1-\eta^2\right)$$

$$\Phi_7(\xi,\eta) = -\sqrt{\frac{3}{32}}\left(1-\xi^2\right)(1+\eta)$$

$$\Phi_8(\xi,\eta) = -\sqrt{\frac{3}{32}}(1-\xi)\left(1-\eta^2\right)$$

Edge (cont.)

$$\Phi_9(\xi,\eta) = -\sqrt{\frac{5}{32}}\,\xi\left(1-\xi^2\right)(1-\eta)$$

$$\Phi_{10}(\xi,\eta) = -\sqrt{\frac{5}{32}}\,\eta(1+\xi)\left(1-\eta^2\right)$$

$$\Phi_{11}(\xi,\eta) = -\sqrt{\frac{5}{32}}\,\xi\left(1-\xi^2\right)(1+\eta)$$

$$\Phi_{12}(\xi,\eta) = -\sqrt{\frac{5}{32}}\,\eta(1-\xi)\left(1-\eta^2\right)$$

$$\Phi_{13}(\xi,\eta) = \sqrt{\frac{7}{512}}\left(1-\xi^2\right)\left(1-5\xi^2\right)(1-\eta)$$

$$\Phi_{14}(\xi,\eta) = \sqrt{\frac{7}{512}}(1+\xi)\left(1-\eta^2\right)\left(1-5\eta^2\right)$$

$$\Phi_{15}(\xi,\eta) = \sqrt{\frac{7}{512}}\left(1-\xi^2\right)\left(1-5\xi^2\right)(1+\eta)$$

$$\Phi_{16}(\xi,\eta) = \sqrt{\frac{7}{512}}(1-\xi)\left(1-\eta^2\right)\left(1-5\eta^2\right)$$

Face

$$\Phi_{17}(\xi,\eta) = \frac{3}{8}\left(1-\xi^2\right)\left(1-\eta^2\right)$$

$$\vdots$$

The specific vertex, edge or face number i with which a shape function Φ_i is associated is shown in Figure 2.4. A graphical representation of the hierarchical truth space shape functions is shown in Figure 2.5.

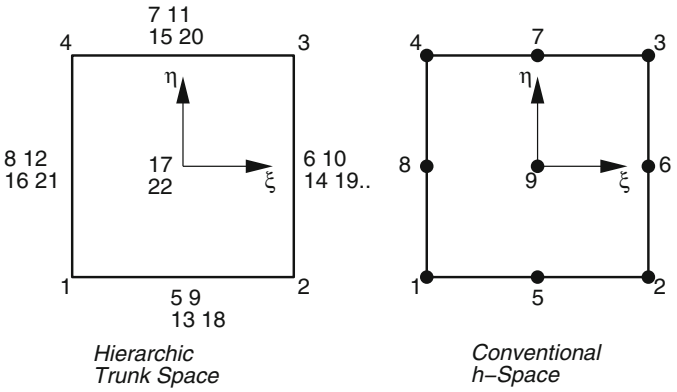

Fig. 2.4 Standard element and notation of shape functions.

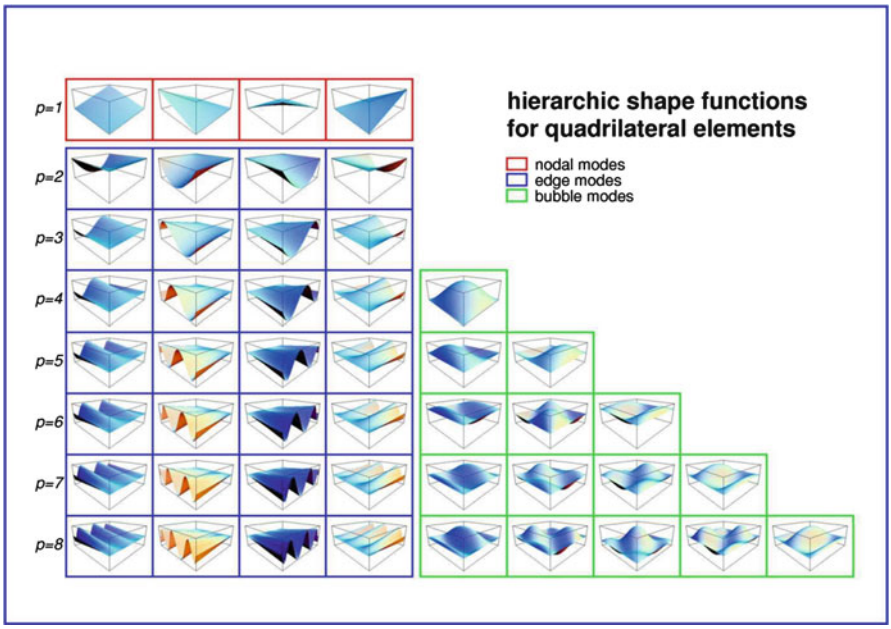

Fig. 2.5 Trunk space hierarchic shape functions over quadrilaterals (from prof. Ernst Rank of TUM-Germany).

For a given mesh and $p-$ level, the global stiffness matrix and load vector are obtained by an assembly procedure of the elemental stiffness matrices and load vectors, so the weak form (2.13) becomes

$$\boldsymbol{c}^T[K]\boldsymbol{b} = \boldsymbol{c}^T\boldsymbol{r}, \quad \forall \boldsymbol{c}, \quad \Rightarrow \quad [K]\boldsymbol{b} = \boldsymbol{r}. \tag{2.24}$$

The solution of (2.24) determines $\boldsymbol{b}$, thus defines the finite element solution τ_{FE} for a given discretization.

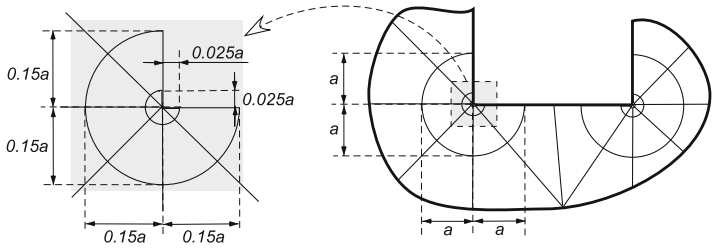

Fig. 2.6 An example of a mesh design with geometric mesh refinement in the vicinity of singular points.

2.2.3 Mesh Design for an Optimal Convergence Rate

For domains with singular points, there exists an optimal design of the discretization in the neighborhood of the singularity: the finite elements should be created so that their sizes decrease in geometric progression towards the singular point, and the polynomial degree over the elements decreases. The optimal *geometric mesh refinement* with a ratio $(\sqrt{2}-1)^2 \approx 0.17$ is applied to the mesh so that $h_{i+1}/h_i = 0.17$, where i increases as the nodes are closer and closer to the singular point. The grading factor is independent of the strength of the singularity, and applicable to both scalar and vector elliptic problems (heat conduction and elasticity). In practice a geometric grading with a factor 0.15 is used, and the generated meshes are called geometric graded meshes. An example for 2-D domains is shown in Figure 2.6.

2.3 Convergence Rates of FEMs and Their Connection to the Regularity of the Exact Solution

The FE solution (τ_{FE} for heat conduction and $\boldsymbol{u}_{\mathrm{FE}}$ for elasticity) is an approximation to the exact solution, and its accuracy depends on the choice of the FE mesh, the polynomial degree assigned to the elements, and the mapping functions. Quantifying this error in energy norm is as important as the FE solution itself, and thus we provide estimates to $\|e\|_{\mathcal{E}(\Omega)} \overset{\text{def}}{=} \|\tau_{\mathrm{EX}} - \tau_{\mathrm{FE}}\|_{\mathcal{E}(\Omega)}$ for heat conduction, or $\|\boldsymbol{e}\|_{\mathcal{E}(\Omega)} \overset{\text{def}}{=} \|\boldsymbol{u}_{\mathrm{EX}} - \boldsymbol{u}_{\mathrm{FE}}\|_{\mathcal{E}(\Omega)}$ for elasticity. The error estimates are presented as error bounds, and are expressed in terms of h, a characteristic length of the largest element in the domain, and p, the polynomial degree of the test and trial functions. Because both h and p are associated with the number of degrees of freedom[1] N, the error bounds are expressed as

$$\|e\|_{\mathcal{E}(\Omega)} \leq C h^n p^m \approx C f(N), \tag{2.25}$$

[1]The connection between h, p, and N depends on the mesh and the dimension of the problem:

where C, n, m are generic constants independent of the discretization parameters and $f(N)$ is a decreasing function of N (see details in [29, Chapter II7] and [14]). The rate at which $f(N) \overset{N\to\infty}{\longrightarrow} 0$ depends on the "regularity" (sometimes also called in the engineering community the "smoothness") of the exact solution (as will be precisely defined in the sequel) in addition to h and p and the FE-extension method (either the h- p- or hp-version).

Definition 2.1. For simplicity consider the heat conduction problem with $k_{ij} = \delta_{ij}$, and instead of the energy norm we use the H^1 norm (these norms are equivalent). Then we say that the bilinear weak form (1.37) has H^s **regularity** if the solution to

$$(\tau, \chi)_{H^1(\Omega)} = (Q, \chi)_{L^2(\Omega)} \qquad \forall \chi \in H^1(\Omega)$$

belongs to $H^s(\Omega)$, i.e., $\tau \in H^s(\Omega)$, for every $Q \in H^{s-2}$ and there exists a constant $c(s, \Omega)$ such that

$$\|\tau\|_{H^s(\Omega)} \leq c(s, \Omega)\|Q\|_{H^{s-2}(\Omega)}.$$

Roughly speaking, the more regular the solution, the less its value and first derivatives change over a given short distance in the domain. Following [176, 178], we may differentiate the solutions of elliptic PDEs based on their regularity into three categories:

- Category A: The exact solution is analytic on each element including on the boundary, $\boldsymbol{u}, \tau \in \mathcal{C}^\infty(\Omega)$.
- Category B: The exact solution is analytic on each element including on the boundary, except at some vertices at which nodes are located (and edges in 3-D domains). *The regularity of the exact solution is determined by the smallest eigenvalue that characterizes the most singular solution in the domain:* $\alpha \overset{\text{def}}{=} \min_i \alpha_i$.
- Category C: The exact solution is neither in category A nor in category B.

A very brief description of the mathematical steps followed to obtain estimates such as (2.25) from various finite element methods (for the heat conduction problem for example) are as follows:

- First bound the error between the function τ and its interpolant $I_h\tau$ in a given norm H^k, in terms of $\|\tau\|_{H^t}$, where $t > k$. That is, provide estimates

$$\|\tau - I_h\tau\|_{H^k(\Omega)} \leq \|\tau\|_{H^t(\Omega)}.$$

$$N = \begin{cases} Ch^{-1}p & \text{for 1-D domains,} \\ Ch^{-2}p^2 & \text{for uniform or radical mesh in 2-D domains,} \\ Ck\rho_o p^2 & \text{for geometric mesh in 2-D domains,} \end{cases} \tag{2.26}$$

where k represents the number of layers and C is a generic constant.

- Second, use regularity theorems (shift theorems), the simplest of which says: *Let the elliptic bilinear form have sufficiently smooth coefficient functions. Then if Ω is convex, the Dirichlet problem is H^2 regular (see definition below). If Ω has a C^s boundary with $s \geq 2$, then the Dirichlet problem is H^s regular.*
- A combination of the first and second steps enables one to bound the interpolation error in terms of a constant depending on the input data (left-hand side of equation and BCs), shape of the boundary, and material coefficients $[k]$.
- The last step is the use of Cea's lemma, bounding the finite element error by the interpolation error:

$$\|\tau - \tau_{\text{FE}}\|_{H^1(\Omega)} \leq \frac{c}{\gamma} \inf_{\chi \in S_h} \|\tau - \chi\|_{H^1(\Omega)}.$$

2.3.1 Algebraic and Exponential Rates of Convergence

The convergence rates represent the speed at which $f(N) \to 0$ as $N \to \infty$. They depend on the FE extension method and the regularity of the exact solution. The two different functions describing $f(N)$ for $N \gg 1$ (termed the asymptotic range) are

$$\text{Algebraic Rate:} \quad \left.\begin{matrix} \|e\|_{\mathcal{E}(\Omega)} \\ \|\boldsymbol{e}\|_{\mathcal{E}(\Omega)} \end{matrix}\right\} \leq \frac{k}{N^{\beta}}, \tag{2.27}$$

$$\text{Exponential Rate:} \quad \left.\begin{matrix} \|e\|_{\mathcal{E}(\Omega)} \\ \|\boldsymbol{e}\|_{\mathcal{E}(\Omega)} \end{matrix}\right\} \leq \frac{k}{\exp\left(\gamma N^{\phi}\right)}; \tag{2.28}$$

$k, \gamma > 0$ are independent of N. The notion of "algebraic rate" of convergence is due to the straight line on a log-log scale obtained by applying the log operator to the convergence estimate (2.27):

$$\log \|e\|_{\mathcal{E}(\Omega)} \leq \log\left(\frac{k}{N^{\beta}}\right). \tag{2.29}$$

For large N the inequality becomes "almost equal," so that (2.29) reads

$$\log \|e\|_{\mathcal{E}(\Omega)} \approx \log k - \beta \log N, \tag{2.30}$$

which is a straight line with slope of $-\beta$, called the "convergence rate."

Depending on the version of the FE method and the regularity of the exact solution, it is possible to estimate the rates of convergence for elliptic problems in 2-D and 3-D as summarized in Tables 2.1 and 2.2 (from [176]).

Table 2.1 Asymptotic rates of convergence in energy norm, two-dimensions.

	Type of Extension		
Category	h	p	hp
A	Algebraic $\beta = p/2$	Exponential $\phi \geq 1/2$	Exponential $\phi \geq 1/2$
B	Algebraic (see Note 1) $\beta = \frac{1}{2}\min(p, \alpha)$	Algebraic $\beta = \alpha$	Exponential $\phi \geq 1/3$
C	Algebraic $\beta > 0$	Algebraic $\beta > 0$	See Note 2

Table 2.2 Asymptotic rates of convergence in energy norm, three-dimensions.

	Type of Extension		
Category	h	p	hp
A	Algebraic $\beta = p/3$	Exponential $\phi \geq 1/3$	Exponential $\phi \geq 1/3$
B	See Note 3		Exponential $\phi \geq 1/5$
C	Algebraic $\beta > 0$	Algebraic $\beta > 0$	See Note 2

Note 1: Uniform or quasiuniform meshes are assumed. The maximum possible value of β obtainable with optimal (adaptively determined) meshes is $p/2$.

Note 2: When the exact solution has a recognizable structure, then nearly exponential convergence rates can be obtained with hp-adaptive schemes [11].

Note 3: The characterization of smoothness in 3-D is much more difficult than in 2-D. Nevertheless, as in the 2-D case, the rate of p-convergence is twice the rate of oh-convergence when quasiuniform meshes are used.

The error in energy norm may be computed by (see [178, p. 69])

$$\left.\begin{matrix} \|e\|_{\mathcal{E}} \\ \|\boldsymbol{e}\|_{\mathcal{E}} \end{matrix}\right\} = \left.\begin{matrix} \sqrt{\frac{1}{2}\mathcal{B}(e,e)} \\ \sqrt{\frac{1}{2}\mathcal{B}(\boldsymbol{e},\boldsymbol{e})} \end{matrix}\right\} = \sqrt{\Pi_{\mathrm{FE}} - \Pi_{\mathrm{EX}}}. \tag{2.31}$$

Although the exact solution is unknown, it is possible to obtain very sharp estimates for the error in energy norm using three consecutive FE solutions with increasing hierarchical spaces having $1 << N_1 < N_2 < N_3$. Combine (2.31) and (2.27) to obtain

$$\Pi_{\mathrm{FE}} - \Pi_{\mathrm{EX}} \approx \frac{k^2}{N^{2\beta}}. \tag{2.32}$$

Table 2.3 Exponential convergence rates in energy norm for $hp-$extensions for 3-D problems having different types of singularities using optimal meshes [75].

extension	Regular	Edge	Edge-Vertex	Vertex
hp	$\phi = 1/3$	$\phi = 1/4$	$\phi = 1/5$	$\phi = 1/4$

The three unknowns $\Pi_{\text{EX}}, k, \beta$ can be computed if we express (2.32) for the three consecutive FE solutions:

$$\Pi_{\text{FE}_i} - \Pi_{\text{EX}} \approx \frac{k^2}{N_i^{2\beta}}, \qquad i = 1, 2, 3. \tag{2.33}$$

These three equations may be solved and one obtains an implicit equation for determining Π_{EX}:

$$\frac{\Pi_{\text{EX}} - \Pi_{\text{FE}_3}}{\Pi_{\text{EX}} - \Pi_{\text{FE}_2}} \approx \left(\frac{\Pi_{\text{EX}} - \Pi_{\text{FE}_2}}{\Pi_{\text{EX}} - \Pi_{\text{FE}_1}} \right)^{\frac{\log N_2 - \log N_1}{\log N_3 - \log N_2}}. \tag{2.34}$$

Problem 2.1. Use (2.33) for three consecutive FE solutions to obtain (2.34).

Once Π_{EX} is determined, the error of each FE solution can be estimated by (2.31). These error estimates are progressively better as N increases.

Some Remarks

Before we present some numerical examples, let us provide some remarks on $hp-$extensions and optimal convergence rates (see Table 2.3 and [14]):

- The optimal convergence rate is achieved by taking a geometric graded mesh with a factor 0.17, and a linear-degree vector $\boldsymbol{p}$ such that $p_j = [(2\alpha) - 1)\, j] + 1$, where j indicates the element at the jth layer away from the singular point.
- For $p-$extensions over a geometric mesh with uniform $p = [(2\alpha) - 1)n]$, where n is the number of layers around the singular point, one still obtains an exponential convergence rate, but the exponent ϕ reduces by a factor of about 0.7.
- It is interesting to note that for the h-extensions, the geometric refinement is not optimal, but the radical one is [14]. Using a radical mesh, when refining further and further one obtains the envelope of the h-p version if the polynomial level on every element is increased linearly as the number of elements is increased.

2.3.1.1 Numerical Examples

The examples discussed in this section were constructed so that the exact solutions are known and used to demonstrate the convergence rates of the $h-$ and $p-$extensions.

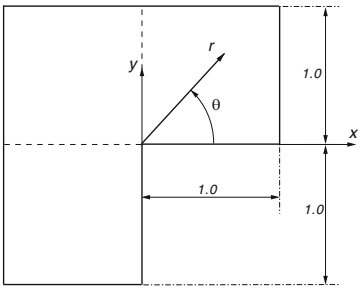

Fig. 2.7 The L-shaped domain (with the coarsest FE mesh having 3 elements).

The Laplace equation over a L-shaped 2-D domain

First, we consider the heat conduction equation in an isotropic material (Laplace equation) $\nabla^2\tau = 0$ over the L-shaped domain in Figure 2.7 (containing a $3\pi/2$ corner) with homogeneous Neumann boundary conditions on the boundaries intersecting at $(x, y) = (0, 0)$, having an exact solution (see (1.11–1.14))

$$\tau_{\mathrm{EX}} = A_1 r^{2/3} \cos\left(\frac{2\theta}{3}\right). \tag{2.35}$$

On the domain's boundaries $x = \pm 1$ and $y = \pm 1$, Neumann boundary conditions according to (2.35) are prescribed:

$$\begin{Bmatrix} \frac{\partial\tau}{\partial x} \\ \frac{\partial\tau}{\partial x} \end{Bmatrix} = \begin{Bmatrix} \frac{\partial\tau}{\partial r}\frac{\partial r}{\partial x} + \frac{\partial\tau}{\partial\theta}\frac{\partial\theta}{\partial x} \\ \frac{\partial\tau}{\partial r}\frac{\partial r}{\partial y} + \frac{\partial\tau}{\partial\theta}\frac{\partial\theta}{\partial y} \end{Bmatrix} = \begin{Bmatrix} \frac{\partial\tau}{\partial r}\cos\theta - \frac{\partial\tau}{\partial\theta}\frac{\sin\theta}{r} \\ \frac{\partial\tau}{\partial r}\sin\theta + \frac{\partial\tau}{\partial\theta}\frac{\cos\theta}{r} \end{Bmatrix} = \frac{2}{3}A_1 r^{-1/3} \begin{Bmatrix} \cos\frac{\theta}{3} \\ \sin\frac{\theta}{3} \end{Bmatrix}. \tag{2.36}$$

The exact potential energy is

$$\Pi_{\mathrm{EX}} = \frac{1}{2}\mathcal{B}(\tau,\tau) - \mathcal{F}(\tau) = -\frac{1}{2}\mathcal{B}(\tau,\tau) = -\frac{1}{2}\iint_{\Omega}\left[\left(\frac{\partial\tau}{\partial x}\right)^2 + \left(\frac{\partial\tau}{\partial y}\right)^2\right] dxdy = -0.91811318807A_1^2. \tag{2.37}$$

Problem 2.2. Use (2.35) and (2.36) to obtain (2.37).

For $h-$extensions with $p = 1$ or $p = 2$ on a uniform mesh, an algebraic convergence is expected with a convergence rate of $-\alpha/2 = -1/3$, whereas a $p-$extension is expected to converge with a convergence rate of $-\alpha = -2/3$. If $p-$extensions on a geometrical graded mesh are performed, an exponential convergence rate is realized for low p-levels, and as the error decreases, the convergence rate may deteriorate to an algebraic rate. In Figure 2.8 we demonstrate numerically the convergence rates that closely match the anticipated theoretical rates for the aforementioned problem with $A_1 = 1$.

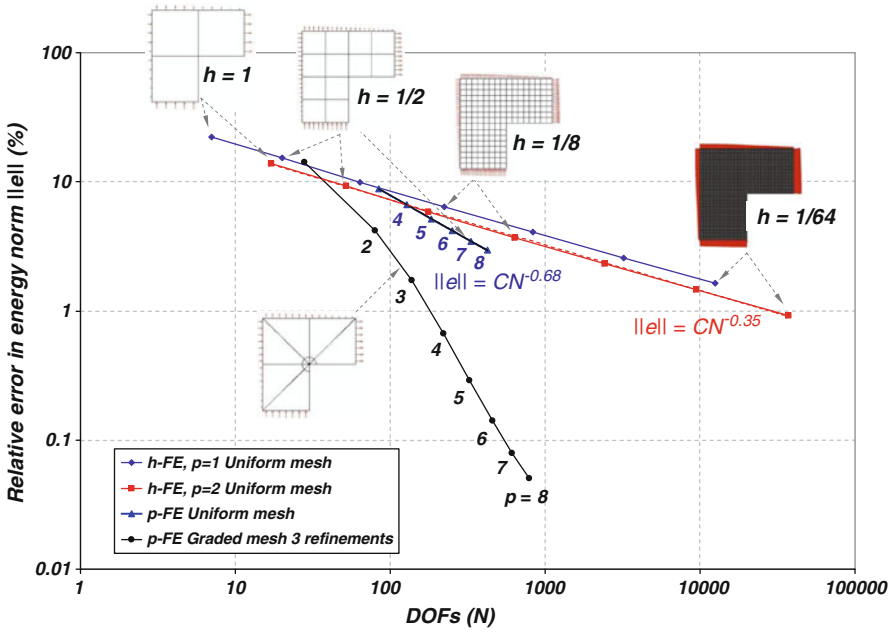

Fig. 2.8 Convergence rates. Heat conduction (Laplace equation).

Elasticity Problem over a L-shaped 2-D Domain

Here we consider the elasticity system over the same L-shaped domain as in the previous example problem rotated by 90° as shown in Figure 6.7 under plane-strain conditions. On the boundaries of the domain, tractions that correspond to the exact "Mode I" stress field in (6.52-6.54) are prescribed, where $A_1 = 1$ and $A_2 = 0$ with $\alpha_1 = 0.5444837368$, and $Q_1 = 0.543075597$ are constants determined so that the solution satisfies the equilibrium equations and the traction-free boundary conditions on the reentrant edges. A Young's modulus $E = 1$ and Poisson ratio $\nu = 0.3$ are chosen so that the exact potential energy for this example problem is given by

$$\Pi_{\text{EX}} = -\frac{1}{2}\mathcal{B}(\boldsymbol{u}, \boldsymbol{u}) = -4.15454423. \tag{2.38}$$

On the 12-quadrilateral uniform mesh ($h = 1/2$) we obtain FE solutions for p ranging from 1 to 8. In addition, we also used h extensions on a sequence of uniformly refined meshes so that h ranges from 1 to 1/16 and fixed $p = 1$ or 2. A strongly graded mesh having three layers of elements with a geometric progression of 0.15 and p ranging from 1 to 8 was also considered. The four convergence paths are shown in Figure 2.9. The algebraic convergence rate of $\approx \alpha = -0.54$ is observed for $p-$extensions over a uniform mesh, and $\approx \alpha/2 = -0.27$ is observed for $h-$extensions. For $p-$extensions over the geometrically graded mesh, a pre-asymptotic exponential convergence rate is realized.

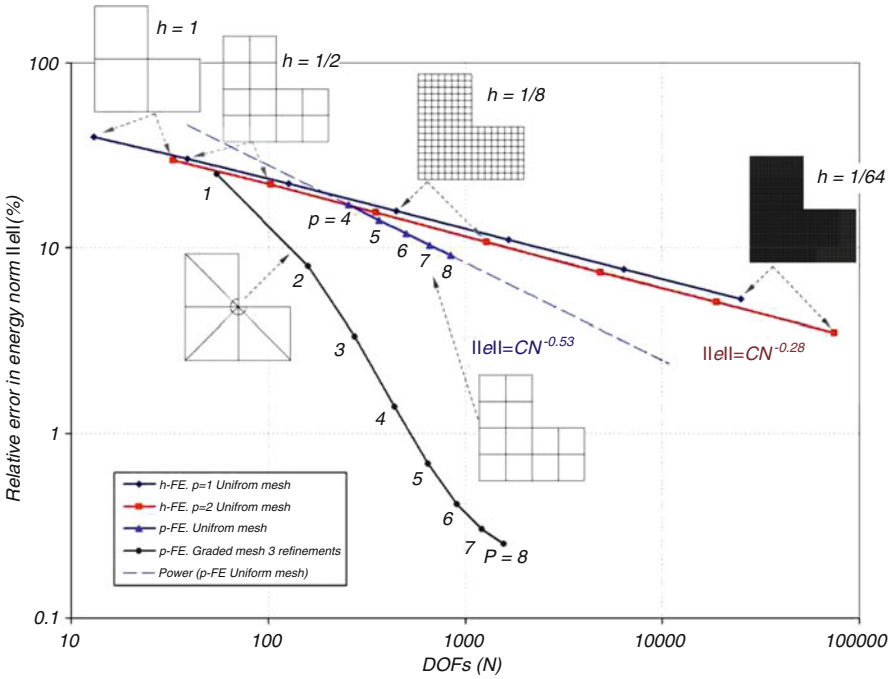

Fig. 2.9 Convergence rates. Elasticity problem over a L-shaped domain.

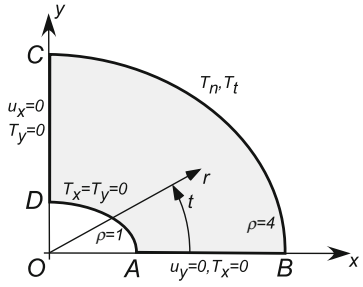

Fig. 2.10 Elliptical domain and boundary conditions for the elasticity problem with an analytical solution.

Elasticity Problem in a 2-D Domain Having an Elliptical/Circular Hole

For problems having an analytical solution (the regularity is as high as required) $p-$Extensions are expected to converge exponentially. To demonstrate this convergence pattern we consider a 2-D plate bounded by two ellipses and the x-y axes shown in Figure 2.10. The inner elliptical boundary AD has major axis $1 + m$ and minor axis $1 - m$, whereas the outer one, BC, has major axis $4 + m/4$ and minor axis $4 - m/4$. One may observe that for $m = 0$ one obtains concentric circles, and as $m \to 1$, the inner ellipse tends to a crack. On the inner elliptical boundary

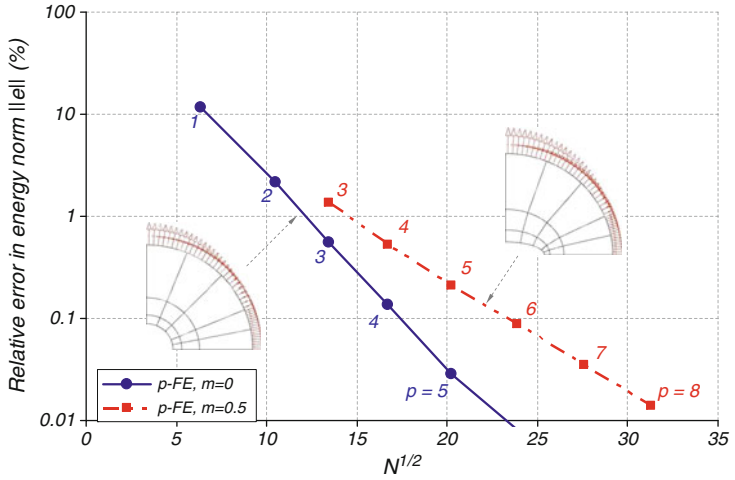

Fig. 2.11 Convergence rates. Elasticity problems with analytical solutions.

AD traction-free conditions are prescribed; on the two straight boundaries AB and DC symmetry boundary conditions are prescribed and on the elliptical boundary BC normal and tangential tractions are prescribed according to (see details in [209])

$$T_t = \frac{1}{g^2(4,\theta(t))}\{\sin 2\theta(t)[480(1+m)(16-m^2)+255(m^2+256)] \\ -4080m\sin 4\theta(t)\}, \tag{2.39}$$

$$T_n = \frac{1}{g^2(4,\theta(t))}\left\{15(256-2m-m^2)(16-m^2)+\cos 2\theta(t)\right. \\ \left.\left[-193(256+m^2)-512(m^2+1)\right]+7200m\cos^2 2\theta(t)\right\}, \tag{2.40}$$

where

$$g(4,\theta(t)) = 256-32m\cos 2\theta(t)+m^2, \quad \text{and} \quad \theta(t) = \arctan\left\{\left(\frac{16+m}{16-m}\right)\tan(t)\right\}.$$

For an isotropic material under the assumption of plane stress with $E = 1$ and $\nu = 0.3$, the following values for the potential energy for the two different m's are obtained: $\Pi_{\text{EX}}(m = 0) = -26.33892955$ and $\Pi_{\text{EX}}(m = 0.5) = -27.08611104$. By varying m from 0 to 0.5, we obtain stress concentration factors at point A that range from 3 to 7, respectively, but the solution is still analytic. A $p-$FE analysis was performed on a mesh of 15 quadrilateral elements by increasing the polynomial order from 1 to 8, where an exponential convergence rate is expected:

$$\|\boldsymbol{e}\|_{\mathcal{E}} \leq \frac{k}{\exp(\gamma N^{\phi})}.$$

Applying the log operator to the convergence estimate (2.28), and since the problem is in Category A, then according to Table 2.2,

$$\log \|\boldsymbol{e}\|_{\mathcal{E}} \leq \log k - \gamma N^{1/2} \log(\exp). \tag{2.41}$$

For large N the inequality becomes "almost equal" and we plot in Figure 2.11 the log of the relative error in energy norm as a function of $N^{1/2}$. As expected, a straight line is obtained both for the domain with $m = 0$ and for $m = 0.5$.

Having described and demonstrated the high convergence rates of the $p-$version of the FEM, we apply it in the next chapters for the computation of the eigenpairs to extract GFIFs and GSIFs.

http://www.springer.com/978-1-4614-1507-7

Singularities in Elliptic Boundary Value Problems and Elasticity and Their Connection with Failure Initiation

Yosibash, Z.

2012, XXII, 462 p., Hardcover
ISBN: 978-1-4614-1507-7